IOPscience iopscience.iop.org

Home Search Collections Journals About Contact us My IOPscience

Positron spectroscopy of vacancy-type defects in Si created by 5 keV B^+ implantation

This article has been downloaded from IOPscience. Please scroll down to see the full text article.

1998 J. Phys.: Condens. Matter 10 10403

(http://iopscience.iop.org/0953-8984/10/46/008)

View the table of contents for this issue, or go to the journal homepage for more

Download details:
IP Address: 171.66.16.151
The article was downloaded on 12/05/2010 at 23:31

Please note that terms and conditions apply.

J. Phys.: Condens. Matter **10** (1998) 10403–10408. Printed in the UK PII: S0953-8984(98)97558-0

Positron spectroscopy of vacancy-type defects in Si created by 5 keV B^+ implantation

F Malik†, P G Coleman†, A P Knights‡, R Gwilliam‡, A Nejim‡ and O Y Ho‡

† School of Physics, University of East Anglia, Norwich NR4 7TJ, UK
‡ School of Electronic Engineering, Information Technology and Mathematics, University of Surrey, Guildford, Surrey GU2 5XH, UK

Received 30 April 1998

Abstract. Structural damage resulting from the implantation of 5 keV B^+ ions into FZ-Si has been investigated by positron annihilation spectroscopy (PAS) using a tuneable monoenergetic beam. Four samples, exposed to ion fluences from 2×10^{12} to 2×10^{15} cm^{-2}, were studied. The PAS results demonstrate the applicability of the technique to the study of vacancy-type defects in small-scale device structures created by very low-energy ion implantation. Ion depth profiles determined by SIMS exhibited tails extending well beyond the limit predicted by the code TRIM, attributed to ion channelling. PAS, when extended by repeated measurements after precise etching of 40 and 140 nm of material via anodic oxidation, showed that the vacancy-type defect depth profiles also extended far beyond the limit predicted by TRIM. The ratio of defects to ions increases with depth, suggesting that the defect tails are not simply correlated to the implanted ions but that there may also be a contribution from post-implantation defect diffusion.

1. Introduction

Ion implantation is the most important tool used for dopant introduction in Si integrated circuit technology. The implantation process creates lattice vacancies, a few per cent of which survive the initial migration and annihilation with interstitials and either coalesce into divacancies [1] or form room temperature impurity–defect complexes [2]. This concentration of residual open-volume defects can affect the performance of devices, and it is thus important to gain as much information about them, and the efficacy of methods for eliminating them, as possible.

Positron annihilation spectroscopy (PAS) using positron beams of controllable energy has proved to be a particularly sensitive method of locating and identifying vacancy-type defects produced by ion implantation, being able to probe samples to depths of $\sim 10^2$ to 10^3 μm, as well as showing sensitivity to defects at concentrations as low as 10^{-7} per atom [3]. This (non-destructive) technique was employed, for example, by Gebauer *et al* to study defects created by boron implantation of silicon at fluences between 10^{14} and 2×10^{16} cm^{-2} and energies of 50, 150 and 300 keV [4].

The computer code TRIM [5] is used widely in the microelectronics industry to predict both ion and vacancy depth profiles following ion implantation. TRIM does not allow for the effects of ion channelling and/or post-implantation diffusion on either distribution. Additionally, the loss of vacancies referred to earlier is not accounted for. The dopant distribution can be determined experimentally via depth profiling by secondary ion mass

0953-8984/98/4610403+06$19.50 © 1998 IOP Publishing Ltd

spectrometry (SIMS) or (in the case of large fluences) Rutherford back-scattering (RBS). PAS offers the ability to profile open-volume defects yielding novel information such as the existence of vacancies to depths beyond—sometimes by a considerable factor—those predicted by TRIM [6, 7].

The continuing quest for ever smaller device structures has the consequence of ion implantation at ever lower energies and fluences. Broadening of the ion profile following post-implantation annealing is therefore becoming increasingly significant. For such shallow implantation, the final dopant profile is strongly affected by the implant induced damage due to defect enhanced diffusion [8].

The purpose of the present study is to investigate the applicability of PAS in characterizing structural damage resulting from the implantation of 5 keV B^+ ions into FZ- (float-zone) Si at fluences as low as 2×10^{12} cm^{-2}. Because the positron implantation profile becomes increasingly extended as the incident positron energy (and hence mean implantation depth) increases, the depth sensitivity of the technique decreases with depth. Furthermore, the fact that the majority of positrons annihilate in vacancies in the large peak just below the surface means that the ability of PAS to study lower-intensity extended vacancy-type defect tails is limited. The authors therefore combine standard non-destructive PAS with etching of known sample thicknesses, extending the idea of Fujinami and Chilton [7] by controlling the etching process via anodic oxidation.

The experimental details are described in section 2, and the results for four samples implanted with different B^+ fluences are presented and discussed in section 3.

2. Experimental details

Four samples were implanted with 5 keV $^{11}B^+$ ions using the Danfysik high current implanter at the University of Surrey. The $^{11}B^+$ ions were extracted with a potential of 30 kV from the ion source and then decelerated by 25 kV at the end of the flight tube. Following the 30 kV extraction lens at the end of the ion source, the ions pass through two stage magnetic analysis producing a high purity ion beam. In the final flight path the beam spot size and shape is defined using water-cooled silicon slits together with a combination of a magnetic and electrostatic quadrupole lenses. Only silicon is used in the slits and the defining aperture to help avoid cross-contamination from forward sputtering of metallic impurities. There is also a neutral trap incorporated in this line. The ion beam is scanned electrostatically using a triangular wave form defined by a 10 MHz Wavetek function generator. The frequencies used were 1 kHz for the X scan and 1004.5 Hz for the Y scan. This produces uniform implants across the wafer to $\pm 2\%$. However, greater non-uniformity is produced in these implants due to the focusing action of the deceleration lens.

The samples were attached to 6 in wafers using photoresist and then mounted on to the deceleration lens housed at the end of the beam line in a vacuum of 10^{-4} Pa. For these implants the wafers were tilted at 7°. Four fluences were implanted -2×10^n cm^{-2}, where $n = 12$, 13, 14 and 15. The instantaneous beam current density was 16 μA cm^{-2}, while the time-averaged beam current density was less than 0.2 μA cm^{-2}.

The four samples were divided for PAS and SIMS measurements.

Controlled-energy PAS was performed using the computer-controlled positron beam at the University of East Anglia (UEA) [9]. A monoenergetic beam of positrons, of energies in the range 0 to 30 keV, impinges upon the sample surface in vacuum conditions ($\sim 10^{-6}$ Pa). The implanted positrons rapidly thermalize and, while diffusing through the material, may be trapped by vacancy-type defects or reach the surface. At each energy the annihilation

gamma photopeak is accumulated by a Ge detector–amplifier–multichannel analyser system. The extent of the Doppler broadening of the peak is characterized by the sharpness, or S, parameter, which is taken as the ratio of counts in the central region to that of the whole peak. Its value is arbitrarily taken as $\sim$0.5 by choosing the limits of the central peak region appropriately although, once set, these limits must remain constant and the peak centroid must be stabilized for any meaningful comparisons to be made. The value of S_D for a positron annihilated when trapped in a vacancy-type defect is typically higher than S_B, for annihilation in a 'free' state in the bulk (e.g. $S_D/S_B \approx 1.035$ for a divacancy in Si [1]) and lower than S_B for annihilation at an oxide-covered Si surface ($S_S/S_B \approx 0.94$). The former is due to the relative absence of higher-momentum (core) electrons in the defect, and the latter reflects annihilations with higher-momentum oxygen electrons. The measured value of S at each E is a linear combination of weighted contributions from S_S, S_D and S_B. The weighting factor for S_D depends upon the defect concentration profile, and this—together with the positron implantation profile [10] and diffusion constant—is fed into the fitting program POSTRAP [12]. Self-consistent fits are obtained for the four samples. The data can be fitted with a simple box defect distribution (i.e. a uniform defect concentration to a given depth below the surface).

As discussed in section 1, the problem of decreasing depth resolution with increasing positron energy is attacked by remeasuring $S(E)$ after controlled etching of known thickness of implanted Si. This is achieved by anodic oxidation of the samples to predetermined depths, followed by etching by hydrofluoric acid. The etching removes the oxidized layer only and leaves the Si surface H terminated, essentially changing the nature of the surface such that S_S approaches S_B. It has been demonstrated experimentally that the etching process does not introduce damage in the surface region to which positrons are sensitive [11]. The tails of the defect distributions for the etched samples are assumed to be exponential in nature and fits were achieved using a set of boxes forming an exponentially decreasing histogram.

3. Results and discussion

Figure 1 shows three adjacent plots of the normalized S-parameter ($=S/S_B$) versus incident positron energy E for the four implanted samples, before and after two etches of 40 nm and a further 100 nm (numbers A1–4, B1–4 and C2–4, respectively). The S_B was obtained from the fits for all four samples and also from data for an unimplanted (virgin) Si reference sample. The virgin Si data also serve to highlight visually the presence of low momentum positron trapping sites, namely open-volume defects formed by the implantation of the boron ions. The data for H-terminated virgin Si after etching of the native oxide by HF are shown in figure 1(c), illustrating the change in the surface S-value and the absence of detectable near-surface open-volume defects created by the etching process.

Looking at the plots A1 to A4 in figure 1(a) it is clear that there are more defects present in the more highly doped samples, with saturation trapping occurring at beam fluences in the range 10^{14} to 10^{15} ions cm^{-3}. The data are also plotted against the mean positron implantation depth using the expression $\bar{z} = 172E^{1.6}$ nm (E in keV) [10]; however, from the plots for the as-implanted samples A1–4 it is not possible—because of the extended positron implantation profile—to judge visually the maximum depth of the open-volume defects. After removal of material by etching of thickness equal to the projected ion range of 40 nm, it is evident that—for samples B2–4—there are still a considerable number of trapping sites present; indeed, the near-surface defects appear still to trap almost all of the positrons, for the measured normalized S-value is close to the 1.035 seen for samples A3

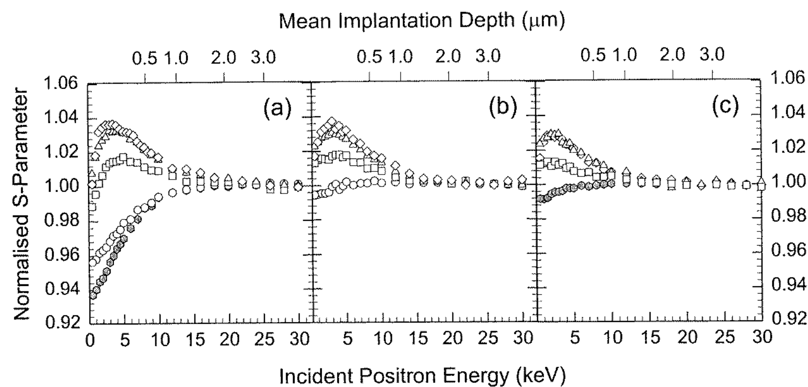

Figure 1. Normalized S-parameter against incident positron energy E for (a) unetched samples (A1–4 plus virgin Si), (b) samples with 40 nm etched (B1–4) and (c) samples with 140 nm etched (C2–4) and virgin Si with native oxide removed by HF etching. Shaded hexagons: virgin Si. Circles: ion fluence 2×10^{12} cm^{-2}. Squares: 2×10^{13} cm^{-2}. Triangles: 2×10^{14} cm^{-2}. Diamonds: 2×10^{15} cm^{-2}.

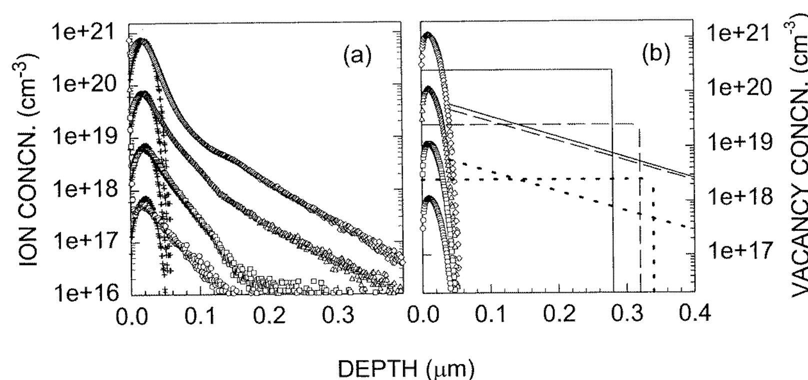

Figure 2. (a) +: TRIM simulations of 5 keV B^+ depth distributions in Si at fluences of 2×10^n cm^{-2}, where n = 12, 13, 14 and 15. Other symbols are SIMS data for the same ion fluences (same symbol convention as figure 1). (b) Symbols (convention as in figure 1): TRIM simulations for vacancy profiles for the four ion fluences, normalized by $\times 0.05$ (see text). Lines show box defect profiles and exponential defect tails fitted by POSTRAP (see text) for ion fluences of 2×10^{15} cm^{-2} (solid), 2×10^{14} cm^{-2} (broken), and 2×10^{13} cm^{-2} (dotted).

and 4. Conversely, any defects left by the etching of sample A1 are at a concentration below that detectable by positrons; this can be seen visually by comparing plot B1 with the plot for the etched virgin sample shown in figure 1(c). Even after the removal of a further 100 nm, we still observe what appears to be close to saturation trapping for samples C3 and 4. Note also that the surface S-parameter value (i.e. at $E = 0$) increases significantly after etching, to close to unity; this is expected to be the case for an H-terminated Si surface [7].

The data for the unetched samples (A2–4) were fitted by assuming single 'box' (uniform) defect distributions (no reliable fitting could be performed for sample A1 because of the low defect concentration). The results are given in table 1. These fits immediately indicate that defects exist at detectable concentrations at depths far below the ion range. To fit the data for the etched samples (except for B1 and C1, whose defect concentrations were below

Table 1. Fitting parameters for unetched samples (A) and those etched by 40 nm (B) and 140 nm (C). See text for definitions of parameters.

Sample set	Defect concentration at surface (cm^{-3})	Depth of distribution (nm)	Decay length (nm)
A2	2.5×10^{18}	340	
A3	2.5×10^{19}	320	
A4	2.5×10^{20}	280	
B2	5.75×10^{18}		120
B3	4.75×10^{19}		120
B4	6.0×10^{19}		115
C2	2.5×10^{18}		120
C3	2.0×10^{19}		120
C4	2.5×10^{19}		115

detectable limits) it was assumed that the defect concentration profile could be described by $C = C_0 \exp(-x/L)$, where C_0 is the initial defect concentration at the 'new' surface ($x = 0$) and L is the decay length. This assumption also includes that of a uniform defect type at all depths. For chosen C_0 and L values an exponential histogram was constructed for insertion into the program POSTRAP, using five blocks. Values used for the specific positron–defect trapping rate and defect S-parameter (S_D) were 5×10^{14} s^{-1} and $\sim$1.035, respectively [1]. Values of L and C_0 were varied until a fit was obtained giving the expected S_D for each of the five bars of the histogram. Fitting was carried out first on the sample set C2–4. It was found that two sets of L and C_0 fitted the experimental curves, both giving reasonable values of S_D but with markedly differing values of L. To ascertain which of the two sets obtained was valid, a self-consistency check was performed by extrapolating back by 100 nm, the amount of the second etch, to calculate C_0 values for fits to the B1–4 data. The results of the exponential fits for both etched samples (B and C) can be found in table 1.

Figure 2(a) shows the implanted ion distributions as measured using SIMS and those calculated by TRIM. The default values for displacement and binding energies were used as input parameters in the latter. The simulated and measured distributions are in agreement over the first 50 nm, after which the two curves diverge. The discrepancy at deeper depths may be attributed to ion channelling not accounted for in the TRIM code.

Figure 2(b) compares the TRIM vacancy distributions with the POSTRAP exponential fits to the data for the etched samples B and C in figure 1 and the single-box fits to the data for the unetched samples A2–4. The average number of vacancy-type defects per ion deduced from the single-box fits is a little over 2, compared with the TRIM result of 40. This suggests that about 95% of the vacancies initially created by the ions disappear via post-implantation migration, recombination and coalescence. The TRIM vacancy distributions in figure 2(b) have thus been multiplied by 0.05 for comparison with experiment. The exponential tails for samples C3 and 4 are, like the raw data, very similar; this is because the concentrations of trapping sites just below 140 nm depth (the amount etched for samples C) are both near the upper limit of discrimination by the PAS technique (corresponding to saturation trapping).

The shapes of the experimental distributions in figures 2(a) and 2(b) are, on first sight, similar; the majority of ions/vacancies are in a peak in the first 50 nm below the surface, followed by low-level exponential tails. However, the ratio of the defect to ion concentration increases with increasing depth, suggesting diffusion of defects away from the surface.

4. Conclusion

PAS has been used in conjunction with controlled etching to study the distribution of open-volume defects created by 5 keV boron ions implanted into Si. There are two main conclusions: (a) PAS is a suitable spectroscopy for studying open-volume defects in structures created by very low energy, relatively low fluence ion implantation, and (b) PAS suggests that defect tails extend to depths beyond those expected from SIMS data on ion tails.

Acknowledgments

The authors are grateful to G Cooke at the Department of Physics, University of Warwick for the SIMS measurements. This work is supported by the EPSRC grant No GR/K56247, under the pump priming scheme.

References

[1] Coffa S, Privitera V, Priolo F, Libertino S and Mannino J 1997 *J. Appl. Phys.* **81** 1639
[2] Kyllesbech Larsen K, Privitera V, Coffa S, Priolo F, Campisano S U and Carnera A 1996 *Phys. Rev. Lett.* **76** 1493
[3] Asoka-Kumar P, Lynn K G and Welch D O 1994 *J. Appl. Phys.* **76** 4935
[4] Gebauer J, Eichler S, Krause-Rehberg R and Polity A 1997 *Appl. Surf. Sci.* **116** 215
[5] Ziegler J F, Biersack J P and Littmark U 1985 *The Stopping and Range of Ions in Solids* (New York: Pergamon)
[6] Knights A P, Carlow G R, Zinke-Allmang M and Simpson P J 1996 *Phys. Rev.* B **54** 13 955
[7] Fujinami M and Chilton N B 1993 *J. Appl. Phys.* **79** 9017
[8] Chason E *et al* 1997 *J. Appl. Phys.* **81** 6513
[9] Chilton N B and Coleman P G 1995 *Meas. Sci. Technol.* **6** 53
[10] Ritley K A, Lynn K G, Ghosh V J, Welch D O and McKeown M 1993 *J. Appl. Phys.* **74** 3479
[11] Nejim A, Knights A P, Jeynes C, Coleman P G and Patel C J 1998 *J. Appl. Phys.* **83** 3565
[12] Aers G 1990 *Positron Beams for Solids and Surfaces* ed P J Schultz, G R Massoumi and P J Simpson (New York: AIP) p 162